ISSN 1027-5495. Functional Materials, 28, No.1 (2021), p. 178-186.
doi:https://doi.org/10.15407/fm28.01.178 © 2021 — STC "Institute for Single Crystals"

Determination of pressure drop in a fixed bed catalytic reactor during ammonia oxidation on nanostructured platinum catalyst

D.Kindzera, V.Atamanyuk, O.Dobrovetska, R.Hosovskyi, R.Havryliv

Institute of Chemistry and Chemistry Technology, Department of Chemical Engineering, Lviv Polytechnic National University, 12 S.Bandery Str., 79013 Lviv, Ukraine

Received June 6, 2020

Nanostructured platinum catalyst has been obtained by an electrochemical method. In order to generate the fixed bed, the catalyst was randomly arranged at the perforated bottom of the reactor; the reactor-to-particle diameter ratio was D/d_p = 24.5. The effect of the increasing gas velocity on the pressure drop in the fixed beds with a length of $35{\cdot}10^{-3}$, $45{\cdot}10^{-3}$, $55{\cdot}10^{-3}$, $65{\cdot}10^{-3}$ and $75{\cdot}10^{-3}$ m, which were generated in the downflow reactor, has been established by an experimental method. Ergan and Darcy-Weisbach equations have been used as the numerical methods to calculate the pressure drops within the Reynolds number range of $312 \le Re \le 1177$. The difference between experimental and calculated values of the pressure drops was found to be increased with an increase in the Reynolds number. On the basis of the experimental results, the equation $\Delta P = 49{\cdot}Re_{exp}^{-0.11}{\cdot}(H/d_e){\cdot}(d_p/D){\cdot}\rho{\cdot}\upsilon^2$ has been proposed, which allows us to calculate theoretically the pressure drop in the downflow fixed bed reactor with the developed catalyst within the Reynolds number range of $312 \le Re_{exp} \le 1177$. The maximum relative error between the experimental and theoretical values does not exceed ±3 %.

Keywords: nanostructured platinum catalyst, fixed bed reactor, pressure drop, low-temperature ammonia oxidation process, hydraulic resistance, similarity criterion, energy costs.

Визначення втрат тиску у каталітичному реакторі стаціонарного шару під час окиснення аміаку на наноструктурованому платиновому каталізаторі. *Д.Кіндзера, В.Атаманюк, О.Добровецька, Р.Госовський, Р.Гаврилів*

Електрохімічним методом отримано наноструктурований платиновий каталізатор, який для формування стаціонарного шару розміщений на перфорованому дні реактора зі співвідношенням діаметрів реактор-частинка D/d_p = 24,5. Експериментальним методом встановлено вплив зростаючої швидкості газу на втрати тиску у стаціонарних шарах довжиною $35{\cdot}10^{-3}$, $45{\cdot}10^{-3}$, $55{\cdot}10^{-3}$, $65{\cdot}10^{-3}$, $75{\cdot}10^{-3}$ м, які сформовані у реакторі стаціонарного шару з низхідним газовим потоком, а рівняння Ергана та Дарсі-Вейсбаха використовувалися в якості чисельних методів для розрахунку втрат тиску у діапазоні чисел Рейнольдса $312 \le Re \le 1177$. Аналіз отриманих результатів показав, що різниця між експериментальними і розрахунковими значеннями втрат тиску збільшується зі збільшенням числа Рейнольдса. На основі узагальнення експериментальних результатів, запропоновано рівняння $\Delta P = 49{\cdot}Re_{exp}^{-0.11}{\cdot}(H/d_e){\cdot}(d_p/D){\cdot}\rho{\cdot}\upsilon^2$, яке дозволяє теоретично розрахувати втрати тиску у реакторі стаціонарного шару з низхідним газовим потоком, що працює на отриманому каталізаторі у діапазоні чисел Рейнольдса $312 \le Re_{exp} \le 1177$. Максимальна відносна похибка між експериментальними і теоретичними значеннями не перевищує ±3 %.

Электрохимическим методом получен наноструктурированный платиновый катализатор, который для формирования стационарного слоя насыпью размещен на перфорированном дне реактора с соотношением диаметров реактор-частица D/d_p = 24,5. Экспериментальным методом установлено влияние увеличения скорости газа на потери давления в неподвижных слоях длиной $35{\cdot}10^{-3}$, $45{\cdot}10^{-3}$, $55{\cdot}10^{-3}$, $65{\cdot}10^{-3}$, $75{\cdot}10^{-3}$ м, сформированных в реакторе стационарного слоя с нисходящим газовым потоком. Уравнения Эргана и Дарси-Вейсбаха использовались в качестве численных методов для расчета потери давления в диапазоне чисел Рейнольдса $312 \le Re \le 1177$. Анализ полученных результатов показал, что разница между экспериментальными и расчетными значениями перепадов давления увеличивается с увеличением числа Рейнольдса. В результате обобщения экспериментальных результатов предложено уравнение $\Delta P = 49{\cdot}Re_{exp}^{-0.11}{\cdot}(H/d_e){\cdot}(d_p/D){\cdot}\rho{\cdot}\upsilon^2$, позволяющее теоретически рассчитать потери давления в реакторе стационарного слоя с нисходящим газовым потоком, работающем на полученном катализаторе в диапазоне чисел Рейнольдса $312 \le Re_{exp} \le 1177$. Максимальная относительная погрешность между экспериментальными и теоретическими значениями не превышает +3 %.

1. Introduction

Nowadays, the synthesis of ammonia and methanol, the reforming of methane with carbon (IV) oxide, the oxidation of ethane, hydrochloric acid and sulfur (IV) oxide, as well as the production of hydrogen by the enriched combustion of heavy fuel oil and waste treatment are carried out in fixed bed catalytic reactors, also called packed bed catalytic reactors [1–9]. These reactors are the most commonly used in large-scale production of chemicals. In the reactors, the continuous phase is a fluid or gas and the porous phase consists of catalytic granules which can be loaded into the reactor as single bed units, multi-bed units, and multitube units [10].

Metallic catalysts are involved in 80 % of the industrial catalytic processes. Among all transition metals, noble metals are of particular interest as the catalysts for large-scale industrial application. Supported metallic catalysts can be used to reduce their cost. The most known catalysts are based on Pt (Ni, Ru, Rh, Pd, Ir) deposited on the metal surface, as well as on TiO_2, γ-Al_2O_3, MgO, SiO_2, CeO_2 and ZrO_2 oxides [11–16]. They have shown high activity in various processes and their behavior depends on several interrelated factors, such as the nature of the metal, the type of support and the characteristics of the metal-support interface [11–16]. In general, oxidation of ammonia (NH_3) in the presence of catalysts takes place with the formation of N_2, N_2O and NO and the resulting product depends on the conditions of the process and the catalyst nature [17, 18]. The development of methods for the synthesis of nitrous oxide (N_2O) as a commercial product, has attracted more and more attention in recent years due to the expansion of its field of application in industry. This is particularly relevant for the oxidation of benzene to phenol ($C_6H_6 + N_2O \rightarrow C_6H_5OH + N_2$) and the oxidation of methane to methanol ($CH_4 + N_2O \rightarrow CH_3OH + N_2$). The catalytic oxidation of ammonia to nitrous oxide (N_2O) at low temperatures (200–400°C) is an efficient technique and it can be intensified by the application of new selective catalysts [19].

The influence of various catalysts on the ammonia oxidation process and production of nitrous oxide was studied by many researchers. The ammonia oxidation to N_2O using the most active catalysts, such as Pt, Co_3O_4, MnO_2 in order to obtain N_2 and N_2O was shown in [20, 21]. It has been found that a number of supported catalysts such as Mn/Bi/Al [22], Mn–Bi–O/α–Al_2O_3 [23] and MnO_x/TiO_2 [24, 25] exhibits high selectivity for N_2O during ammonia oxidation.

Catalysts based on Pt exhibit high activity in low-temperature ammonia oxidation and high selectivity for N_2O (NH_3 oxidation begins at 195°C) [21]. The mechanisms of ammonia oxidation using different types of Pt catalysts (single crystals, wires, gauzes and supported catalysts) and the factors controlling the product distribution, i.e. the formation of NO, N_2O and N_2, were studied in [26–28]. It was mentioned [29–32], that Pt states could be efficiently changed by the support material due to the metal-support interaction, and resulted in different catalytic characteristics.

The technology of obtaining nanostructured catalysts attracts the special attention of researchers due to the high activity of the catalysts, in particular, in chemical and electrochemical processes [33, 34]. Metallic supported platinum catalysts may be of interest due to their low cost, high mechanical strength, activity, selectivity and stability. These characteristics are intrinsic to Pt/Me

catalysts, in which Pt is deposited by the electrochemical method on the metal support. Moreover, the electrochemical method ensures the formation of Pt nanoparticles (PtNPs) on the metal support and allows varying the thickness of the coating to provide the formation of a uniform deposited Pt layer [35, 36]. The catalysts are characterized by high adhesion of Pt with the metal substrate, which in turn provides a longer lifetime. Therefore, the nanostructured platinum catalysts obtained by the electrochemical method are promising and their application will provide the intensification of the ammonia oxidation process in the fixed bed reactor.

Apart from the intensification of the ammonia oxidation process by using effective catalysts with long lifetime, it is important to minimize a pressure drop ΔP caused by a hydraulic resistance of the catalyst layers when the reactants are passing through them. The pressure drop is an effective hydrodynamic parameter and an important characteristic of the reactor. It is crucial for the reactors operation and design, as well as for economic reasons, especially for the assessment of operation costs [37–40]. Taking into account that a wide range of the fixed bed equipment such as cooling devices [41, 42], absorption and desorption columns [43, 44], nuclear reactors [45, 46], filtration dryers [47–49] are used for industrial purposes, an additional attention have to be focused on the comprehensive study of the pressure drop by using experimental and numerical methods. From the standpoint of chemical engineering it is also important to know how to minimize the pressure drop and simultaneously to maximize the equipment efficiency and productivity.

Generally, the pressure drop is a function of bed characteristics such as bed length, diameter of particles, porosity and pore distribution, as well as fluid (gas) characteristics such as viscosity, density, and flow rate. Ergun's equation remains the most popular for determining pressure drop although it is applicable only for $Re < 1000$ and does not take into account particle roughness or wall effect [50, 51]. As regards the upflow and downflow fixed bed reactors, there are some differences which can influence the pressure drop. First of all, it is a flow rate which is limited in the upflow fixed bed reactors because of fluidization. In many cases, in order to increase the rate, the catalysts should be covered by a grid but this constructive solution increases the hydraulic resistance of the catalytic layer. Secondly, there are differences in the flow structures at the inlet of the catalyst bed. In the upflow fixed bed reactors the fluid passes through a set of perforations at the bottom (or in the grid) before entering the fixed bed. Thus, a continuous gas flow is divided into separate streams and the structure of the flow before entering the catalytic layer is affected by the characteristics of the perforated bottom or grid. In the case of downflow fixed bed reactors, the formation of such structure is influenced by the characteristics of the fixed bed.

The aim of this work is to determine the pressure drop in the downflow fixed bed reactor with a nanostructured platinum catalyst, which operates at high Reynolds numbers, in order to evaluate the feasibility of transferring the results to a large-scale industrial reactor and to predict the energy costs.

2. Experimental

2.1 Catalyst preparation

The preparation of nanostructured platinum catalyst was carried out according to the method proposed in [52]. In electrolysis, an organic aprotic solvent DMSO (DMSO, 99 %, AlfaAesar), tetrabutylammonium perchlorate (Bu_4NClO_4, ≥99.0 %, Sigma Aldrich) and a reducing metal chloride salt ($PtCl_2$, 99.9 % AlfaAzar) were used. The composition of the prepared solution was as follows: 4 mM $PtCl_2$ + 50 mM Bu_4NClO_4 + DMSO [52].

Steel balls (St3 grade) with a diameter of 4 mm were selected as supports for the formation of PtNPs (Pt nanoparticles). The steel was chosen as the support due to its high adhesion to Pt, which provides a long catalyst life. The round shape and diameter of 4 mm were chosen taking into account the large active surface area of the particles and the acceptable pressure drop in the fixed beds formed by such particles during the passage of reagents through them.

Steel balls and a platinum plate were used as working and counter electrodes, respectively. A silver chloride electrode Ag/AgCl prepared in the saturated KCl solution was used as a reference electrode. Before each experiment, the steel balls were degreased in an aqueous solution of detergent (50-70 g/l) at the temperature of 70°C and washed in flowing and distilled water. The surface was etched in an aqueous solution of the composition g/l: H_2SO_4 — 100, HCl — 15 at room temperature. After that,

the surface of the working electrodes was washed at first with flowing water, then distilled water, isopropanol and dried with hot air.

Electrochemical deposition of platinum nanoparticles was carried out in the range of potentials −0.8...−2.2 V [52]. After the ending of experiment the balls with deposited PtNPs were washed with DMSO, then with isopropanol and dried with hot air.

The nanostructured platinum catalyst (the thickness of the Pt layer is 30–60 nm), which is represented in Fig. 1, is characterized by high adhesion of platinum with the steel support, which provides high mechanical strength and long service life. Due to its high activity in the ammonia oxidation process and selectivity to N_2O, the platinum catalyst can be used for the intensification of the process, as well as for the synthesis of nitrous oxide as a commercial product. This type of catalyst can be also successfully used for other catalytic processes.

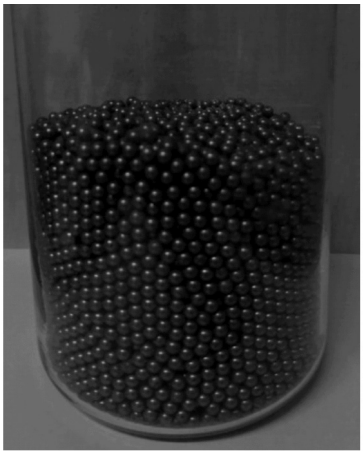

Fig. 1. Nanostructured platinum catalyst obtained on the surface of steel balls.

2.2 Fixed bed formation

To generate a fixed bed, a reactor (9) with an internal diameter of 97 mm used as the main part of the experimental setup is represented in Fig. 2. The support of the reactor was made of aluminum and equipped with a duralumin perforated bottom and an insulating fluoroplastic insert to eliminate heat loss through the walls. The reactor was randomly filled by a nanostructured platinum catalyst (as the most realistic model). To ensure a uniform distribution of the flow over the diameter of the fixed bed and to limit the effect of bypassing, the packing was created with the ratio of the diameter of the reactor particles to the diameter of the catalyst particles $D/d_p = 24.5$. The parameters of the fixed bed were as follows: porosity $\varepsilon = 0.385$ m^3/m^3, the specific surface area $a = 922.53$ m^2/m^3 and the equivalent diameter of the channels $d_e = 1.669 \cdot 10^{-3}$ m.

2.3 Pressure drop evaluation

The experimental method is most convincing for determining the pressure drop. This includes creating suitable fixed bed geometry, pumping a gas flow through it, and using pressure gauges to measure the inlet and outlet pressures of the fixed bed. The experimental setup for the catalytic oxidation of ammonia, as well as physical modeling of the gas flow through the fixed bed is shown in Fig. 2.

Thus, according to the scheme (Fig. 2), an air flow from a gas cylinder (1) and an ammonia flow from the gas cylinder (4) are supplied to a gas mixer (7). By means of gas reducers (2) and (5), the gas flow consumption is set up and registered by electronic flow-meters RPF-I (3) and (6). The mixed gas flow was heated to 473 K±0.5 K in a heater and supplied to the fixed bed reactor (9) in which it was homogeneously distributed over the fixed bed cross-section by a distributor installed at the top of the equipment. The constant temperature at the fixed bed inlet was controlled using a thermal regulator RT-100 and a chromel-copel thermocouple.

The experiments were carried out for the fixed beds length of $35 \cdot 10^{-3}$, $45 \cdot 10^{-3}$, $55 \cdot 10^{-3}$, $65 \cdot 10^{-3}$ and $75 \cdot 10^{-3}$ m. To determine the pressures at the inlet and outlet of the fixed bed, electronic gauges DV250A (8) and (10) with an accuracy of ±0.1 Pa were used. The pressure drop was defined as the difference between numerical values. The consumption of the outlet gas flow was registered by an electronic flow-meter RPF-I (11). The experiments were carried out at superficial velocities ranging from 0.01 m/s to 1.78 m/s. After passing through the fixed bed reactor (9), the outlet gas flow was supplied to the gas cylinder (13) by a compressor (12). Every experiment was carried out three times to obtain the reliable data.

For determination of the pressure drop in fixed beds consisting of spherical particles, Ergun's equation is recommended; according to this, the pressure drop is simultaneously caused by both inertial and viscous components [53, 54]:

$$\frac{\Delta P}{H} = 150 \frac{\mu \cdot (1-\varepsilon)^2}{d_p^2 \varepsilon^3} \upsilon_0 + 1.75 \frac{\rho \cdot (1-\varepsilon)}{d_p \cdot \varepsilon^3} \upsilon_0^2 \quad (1)$$

in which H is the fixed bed length (m); υ_0 is the superficial fluid velocity (m/s); μ is

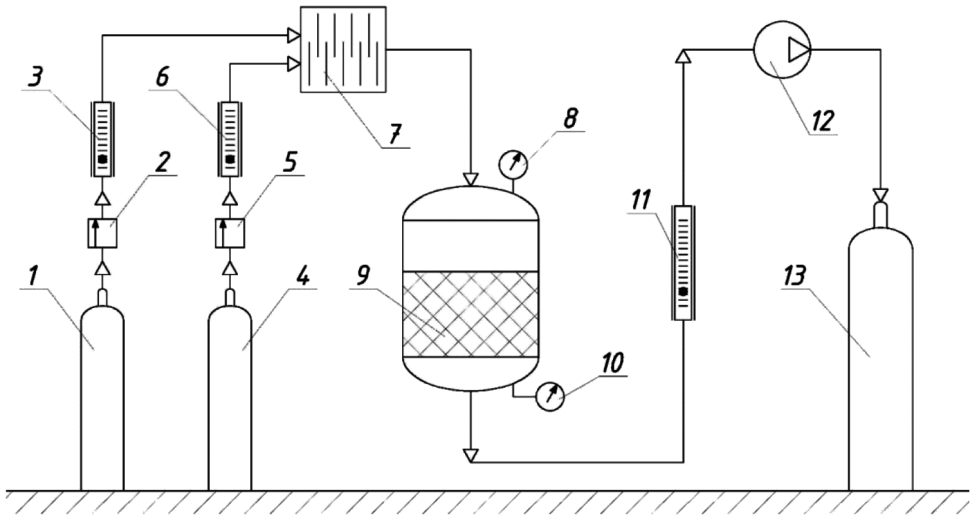

Fig. 2. Scheme of the experimental setup: *1*, *4*, *13* — gas cylinders; *2*, *5* — gas reducers; *3*, *6*, *11* — electronic flow meters RPF-I; *7* — gas mixer; *8*, *10* — electronic pressure gauges DV250A; *9* — fixed bed reactor; *12* — compressor.

the fluid viscosity (Pa·s); ε is the porosity; d_p is the particle diameter (m); ρ is the fluid density (kg/m^3).

Darcy-Weissbach is another famous equation to predict the pressure drop [55]:

$$\Delta P = \lambda \cdot \frac{H_e}{d_e} \cdot \frac{\rho \cdot \upsilon_0^2}{2}. \qquad (2)$$

In comparison to Eq. (1), this is focused on the applicability of the resistance coefficient λ which indicates the loss of pressure through friction; in the case of a fixed bed formed by round particles, it can be determined as $\lambda = 133/Re + 2.34$; d_e is the equivalent diameter and $H_e = 1.5 \cdot H$ is the equivalent length of channels, where H is the fixed bed length.

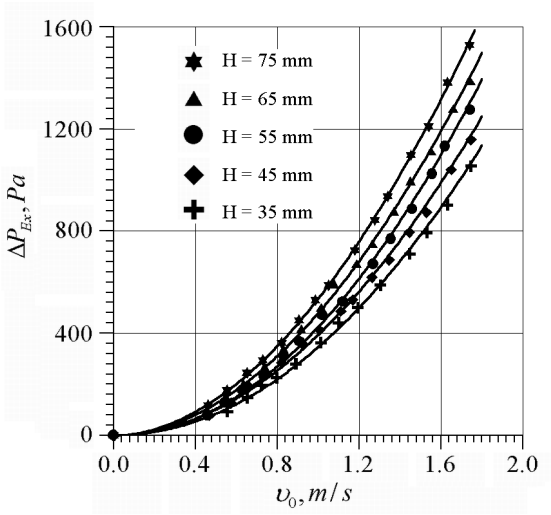

Fig. 3. The pressure drop in fixed beds of different length vs. gas superficial velocity.

3. Results and discussion

3.1 Experimental results of the pressure drop evaluation

The experimental setup shown in Fig. 2 was used to measure the pressure drops in the fixed beds made of nanostructured platinum catalyst. According to the experimental procedure described in Section 2, the pressure drops were measured for the fixed beds with lengths of $35 \cdot 10^{-3}$, $45 \cdot 10^{-3}$, $55 \cdot 10^{-3}$, $65 \cdot 10^{-3}$ and $75 \cdot 10^{-3}$ m; the experimental curves are presented in Fig. 3.

In general, Fig. 3 demonstrates that an increase in the gas superficial velocity increases the pressure drop in the fixed beds. The effect of the length of the fixed beds on the pressure drop is significant and, as an example, it is evident from Fig. 3, that at the actual velocity of 1.78 m/s, the pressure drop changes from 985 Pa (for the length of the fixed bed H = $35 \cdot 10^{-3}$ m) to 1530 Pa (for the length of the fixed bed H = $75 \cdot 10^{-3}$ m). The graphs shown in Fig. 3 have practical application and allow determining the values of the pressure drops in the fixed beds of various lengths for the required values of the gas superficial velocity; this is important for forecasting energy costs at the equipment design stage.

Table. Pressure drop in the fixed bed of the length $H = 75 \cdot 10^{-3}$ m

Superficial gas velocity, υ_0, m/s	Actual gas velocity, υ_0, m/s	Reynolds number, Re	Experimental pressure drop ΔP_{Ex}, Pa	Pressure drop according to Ergun's equation, ΔP_{Ergun}, Pa	Relative error, ΔP_{Ergun}	Pressure drop according to Darcy-Weisbach's equation, ΔP_{Darcy}, Pa	Relative error, δ_{Darcy}
1.74	4.52	1177	1529.837	1439.523	5.90	1355.703	11.38
1.63	4.24	1104	1382.738	1275.129	7.78	1196.294	13.48
1.54	3.99	1041	1211.121	1142.833	5.64	1068.27	11.79
1.45	3.74219	983	1098.345	1024.774	6.70	954.2555	13.12
1.34	3.48	906	936.5351	880.2275	6.01	815.0193	12.98
1.28	3.31	863	843.3719	803.7247	4.70	741.5175	12.08
1.18	3.06	797	725.6921	693.5253	4.43	635.9225	12.371
1.05	2.73	711	588.399	561.4684	4.58	509.9283	13.34
0.99	2.56	666	529.5591	498.9885	5.77	450.5795	14.91
0.91	2.35	613	451.1059	427.9242	5.14	383.3376	15.02
0.82	2.13	555	362.8461	358.0803	1.31	317.5881	12.47
0.73	1.89	493	294.1995	289.3561	1.64	253.3197	13.89
0.65	1.69	440	245.1663	236.8425	3.39	204.5926	16.55

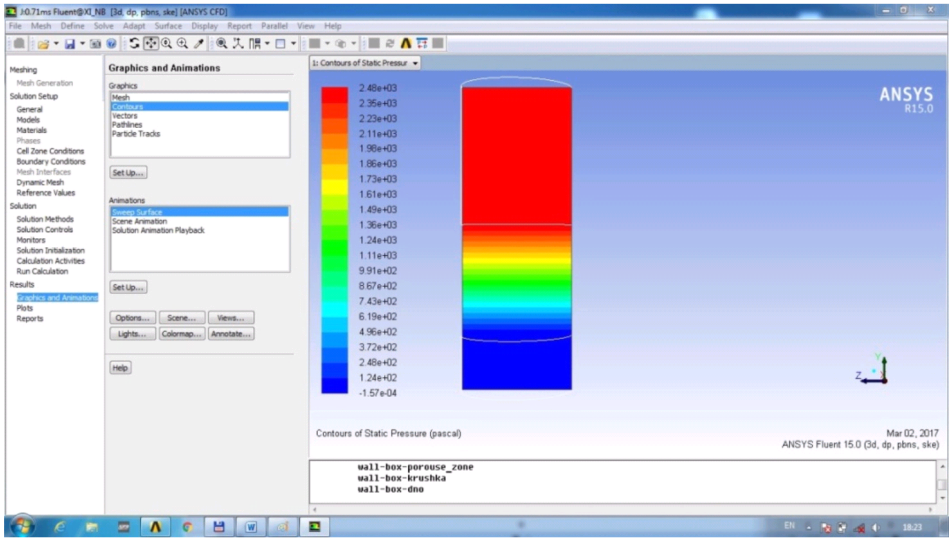

Fig. 4. Contours of static pressure drop in the vertical cross-section of the fixed bed with length $H = 75 \cdot 10^{-3}$ m.

3.2 Numerical results of the pressure drop evaluation

To determine the pressure drop in the fixed beds of different length when passing the gas flow through them, Ergan's equation (1) and Darcy-Weisbach's equation (2) were used. The experimental data and calculation results are presented in Table for the length of the fixed bed $H = 75 \cdot 10^{-3}$ m, as an example. Computational Fluid Dynamics (CFD) has been used to visualize the results in order to obtain the pressure distribution in the vertical cross-section of the fixed bed over the total length $H = 75 \cdot 10^{-3}$ (Fig. 4). For the numerical simulation, the ANSYS FLUENT 17 software was used. CFD simulation was carried out in several steps: creating the geometry of a 3D model, creating a computational mesh, developing a CFD model with appropriate boundary condi-

tions, modeling and analyzing the simulation results. All geometric transformations were done in a software module Design Modeler, and the mesh was created in the ANSYS Meshing. The Porous Media Model presented in the ANSYS Fluent software was used to simulate the flow field inside the fixed bed. In addition to the standard flow equations (mass- and continuity conservation equations) the flow through homogeneous porous media was modeled by adding an extra momentum source term based on the Darsy Law and the force of inertia. The viscous resistance coefficient and the inertial resistance coefficient have been obtained based on experimental results to determine the properties of a porous medium in ANSYS Fluent. The "Realizable" k–ε model was used for modeling the effect of turbulence on flow field velocities [56].

To visualize and to compare the results (Table), the graphs were plotted (Fig. 5).

So, Ergan's equation allows us to predict accurately the pressure drop in the fixed bed up to the Reynolds number of 850, but with an increase in the Reynolds number above 850, the difference between experimental and calculated values increases due to an increased gas turbulence in the channels between particles of the catalyst (Fig. 5), when the effect of the inertial component increases and the effect of the viscous component decreases. In addition, equations (1) and (2) do not take into account the wall effect, which can be conditionally represented as the reactor to catalyst particle diameter ratio D/d_p, as well as the structure of the flow at the entrance to the catalyst bed in the case of a downward gas flow.

3.3 Generalization of the results

Given that the calculated values of the pressure drop for higher Reynolds numbers are not in a good agreement with the experimental ones, it would be useful to generalize the experimental results to estimate the equation which allows the theoretical calculation of the pressure drop in a downflow fixed bed reactor with a new catalyst operating at high Reynolds numbers.

Using the methods of similarity theory, the dependence of the pressure drop on many factors can be represented in the form of compact relationships between dimensionless parameters, known as similarity criteria. So, the experimental data were generalized in accordance with Eq. (3) [55]:

$$Eu = f(Re_{exp}, G_1, G_2), \qquad (3)$$

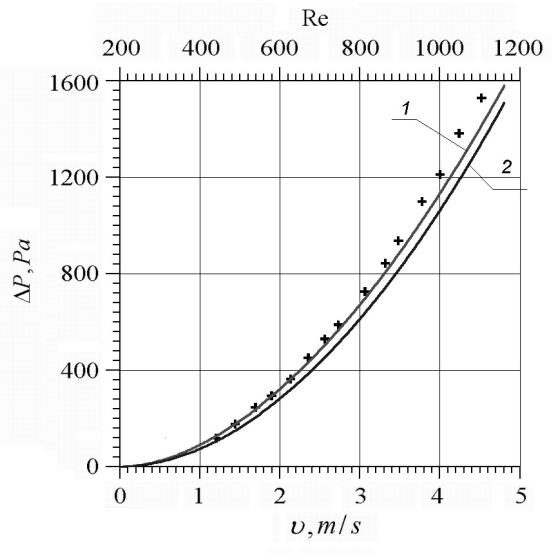

Fig. 5. Pressure drops in the fixed bed of the length $H = 75{\cdot}10^{-3}$ m versus actual gas velocities within the Reynolds number range of $312 \le Re \le 1177$: + — experimental data ΔP_{Ex}, Pa; *1* — calculated results by using Eq. (1), ΔP_{Ergun}, Pa; *2* — calculated results by using Eq. (2), ΔP_{Darcy}, Pa.

$$Eu = A \cdot \mathrm{Re}_{\mathrm{exp}}^{x} G_1^{n} \cdot G_2^{m}, \qquad (4)$$

where $Eu = \Delta P/\rho{\cdot}\upsilon^2$, $Re_{exp} = (\upsilon \cdot d_e{\cdot}\rho)/\mu$ are Euler and Reynolds numbers, respectively; $G_1 = H/d_e$ is the geometric simplex, which represents the ratio of the fixed bed length to the equivalent diameter of the channels; $G_2 = d_p/D$ is the geometric simplex, which represents the ratio of the catalyst particle to reactor diameter.

The values of the coefficient A and exponents x, n and m should be experimentally determined. To determine the coefficient A and exponent x in Eq. (4), the experimental data (for the fixed bed of the length $H = 75{\cdot}10^{-3}$ m) were plotted as the dependence $Eu = f(Re_{exp})$ in the logarithmic coordinates (Fig. 6).

The values of the coefficient A and exponent x were obtained as $A = 49$ and $x = -0.11$. Therefore, taking into account the values of A and x, Eq. (4) takes a form:

$$Eu = 49 \cdot \mathrm{Re}_{\mathrm{exp}}^{-0.11} \cdot \frac{H_e}{d_e} \cdot \frac{d_p}{D}. \qquad (5)$$

Since the Euler number includes the value of the pressure drop, the Eq. (5) may be represented as:

$$\Delta P = 49 \cdot \mathrm{Re}_{\mathrm{exp}}^{-0.11} \cdot \left(\frac{H_e}{d_e}\right) \cdot \left(\frac{d_p}{D}\right) \cdot \rho \cdot \upsilon^2. \qquad (6)$$

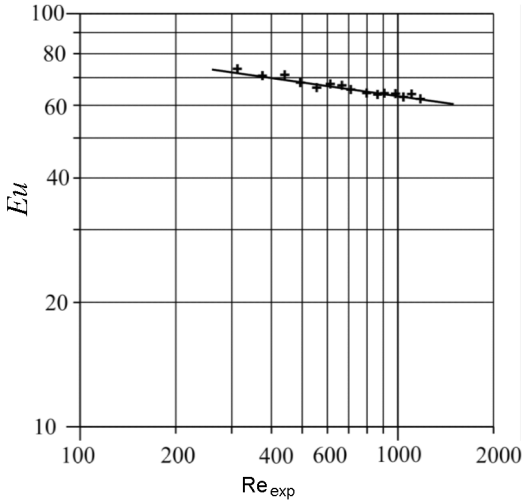

Fig. 6. Generalization of the experimental results: Euler vs. Reynolds number.

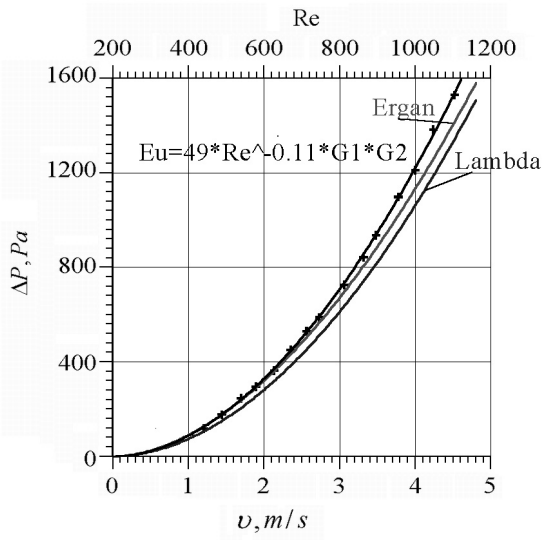

Fig. 7. Pressure drops in the fixed bed of the length $H = 75 \cdot 10^{-3}$ m versus actual gas velocities within the Reynolds number range of $312 \le Re \le 1177$: + — calculated results by using Eq. (6); *1* — calculated results by using Eq. (1), ΔP_{Ergun}, Pa; *2* — calculated results by using Eq. (2), ΔP_{Darcy}, Pa.

The graphs in Fig. 7 compare the results of calculations by Eqs. (1) and (2) with the results obtained using Eq. (6).

Graphic dependencies in Fig. 7 show that the values of the pressure drop obtained by Eq. (6) accurately describe the experimental data (Fig. 5). The maximum relative discrepancy between the experimental and theoretical values does not exceed ±3 %. Therefore, the proposed equation (6) allows us to accurately calculate the pressure drop in a fixed bed reactor with a downward flow in the range of Reynolds numbers $312 \le Re_{exp} \le 1177$. Eq. (6) can be used in the design of industrial fixed bed reactors under conditions of equality of the similarity criteria and geometric simplices.

4. Conclusions

In a downflow fixed bed reactor, the effect of an increase in the gas velocity on the pressure drop in fixed beds of a nanostructured platinum catalyst $35 \cdot 10^{-3}$, $45 \cdot 10^{-3}$, $55 \cdot 10^{-3}$, $65 \cdot 10^{-3}$ and $75 \cdot 10^{-3}$ m long has been experimentally established. The Ergan and Darcy-Weisbach equations have been used for numerical calculations of the pressure drops; the graphs have been plotted to compare the results with experimental data (Fig. 3). The discrepancy between the theoretical and experimental values of pressure drops was found to be increased at Reynolds number above 850.

Generalizing the experimental results, the equation $\Delta P = 49 \cdot Re_{exp}^{-0.11} \cdot (H/d_e) \cdot (d_p/D) \cdot \rho\upsilon^2$ has been proposed which allows with high accuracy theoretically calculating the pressure drop in the downflow fixed bed reactor with new catalyst within Reynolds number range of $312 \le Re_{exp} \le 1177$. The maximum relative discrepancy between experimental and theoretical values does not exceed ±3 %.

References

1. K.C.Sandeep, S.Mohan, D.Mandal et al., *Chem. Engin, Sci.*, **202**, 508 (2019).
2. Z.Sun, D.H.West, V.Balakotaiah, *Chem. Engin. J.*, **377**, 119765 (2019).
3. J.Gomez, J.P.Mmbaga, R.E.Hayes et al., *Int. J. Hydrogen Energy*, **43**, 2677 (2018).
4. G.Boccardo, R.Sethi, D.L.Marchisio, *Chem. Engin. Sci.*, **198**, 290 (2019).
5. E.Afabor, A.Salama, H.Ibrahim, *J. Environ. Chem. Engin.*, **5**, 4850 (2017).
6. M.H.Abdel-Aziz, I.Nirdosh, G.H.Sedahmed, *Int. J. Heat Mass Transfer*, **90**, 427 (2015).
7. F.Obeid, J.Zeaiter, A.H.Al-Muhtaseb et al., *Energy Conver. Manag.*, **85**, 1 (2014).
8. L.Zhang, Sh.Wu, Z.Liang et al., *Chin. J. Chem. Engin.*, **25**, 175 (2017).
9. A.D.Ballarini, S.R.de Miguel, E.L.Jablonski et al., *Catal. Today*, **107**, 481 (2005).
10. M.Bazmi, S.H.Hashemabadi, M.Bayat, *Korean J. Chem. Eng.*, **28**, 1340 (2011).
11. K.Tao, Y.Zhanga, S.Terao et al., *Catal. Today*, **153**, 150 (2010).
12. K.J.Puolakka, S.Juutilainen, A.O.I.Krause, *Catal. Today*, **115**, 217 (2006).
13. F.Pompeo, N.N.Nichio, M.M.V.M.Souza et al, *Appl. Catal. A: General*, **316**, 175 (2007).

14. M.M.V.M.Souza, Martin Schmal, *Appl. Catal. A: General*, **255**, 83 (2003).
15. Y.Takahashi, T.Yamazaki, *Fuel*, **102**, 239 (2012).
16. A.Cherif, R.Nebbali, *Int. J. Hydrogen Energy*, **44**, 22455 (2019).
17. O.N.Bliznjyk, V.V.Prezhdo, *Polish J. Appl. Chem.*, **47**, 65 (2003).
18. M.V.Manna, P.Sabia, R.Ragucci et al., *Fuel*, **264**, 116768 (2020).
19. N.Yu.Masalitina, Ph.D.Thesis, National Technical "Kharkiv Polytechnical Institute", Ukraine, Kharkiv (2017).
20. Y.Luo, Y.Shi, S.Liao et al., *J. Power Sourc.*, **423**, 125 (2019).
21. H.Ma, W.F.Schneider, *J. Catal.*, **383**, 322 (2020).
22. A.S.Noskov, I.A.Zolotarskii, S.A.Pokrovskaya et al., *Chem. Engin. J.*, **91**, 235 (2003).
23. A.S.Ivanova, E.M.Slavinskaya, V.V.Mokrinskii et al., *J. Catal.*, **221**, 213 (2004).
24. Sh.Hui, Q.Yao, D.Wang et al., *Energy Procedia*, **158**, 1497 (2019).
25. D.Wang, Q.Yao, Ch.Mou et al., *Fuel*, **254**, 115719 (2019).
26. M.Baerns, R.Imbihl, V.A.Kondratenko et al., *J. Catal.*, **232**, 226 (2005).
27. J.Perez-Ramirez, E.V.Kondratenko, V.A.Kondratenko et al., *J. Catal.*, **227**, 90 (2004).
28. J.Perez-Ramirez, E.V.Kondratenko, V.A.Kondratenko et al., *J. Catal.*, 229, 303 (2005).
29. A.Lewera, L.Timperman, A.Roguska et al., *J. Phys. Chem. C*, 115, 20153 (2011).
30. K.Kunimori, Y.Ikeda, M.Soma et al., *J. Catal.*, **79**, 185 (1983).
31. A.K.Datye, D.S.Kalakkad, M.H.Yao et al., *J. Catal.*, **155**, 148 (1995).
32. M.Sun, J.Liu, C.Song et al., *ACS Appl. Mater. Interfaces*, **11**, 23102 (2019).
33. E.Fratini, A.Girella, I.Saldan et al., *Mater. Lett.*, **161**, 263 (2015).
34. I.Saldan, A.Girella, C.Milanese et al., *Functional Materials*, **25**, 82 (2018).
35. Y.Xue, F.Scaglione, P.Rizzi et al., *Appl. Surf. Sci.*, **476**, 412 (2019).
36. A.G.Munoz, H.J.Lewerenz, *J. Electrochem. Soc.*, **156**, D242 (2009).
37. A.Pavlisic, R.Ceglar, A.Pohar et al., *Powder Technology*, **328**, 130 (2018).
38. A.K.Giri, S.K.Majumder, *Chem. Engin.. Res.Design*, **92**, 34 (2014).
39. Z.Guo, Z.Sun, N.Zhang et al., *Chem. Engineer. Sci.*, **209**, 115200 (2019).
40. Ch.J.Dittrich, *Chem. Engineer. J.*, **381**, 122492 (2020).
41. R.Wu, Y.Fan, T.Hong et al., *Appl. Thermal Engineer.*, **162**, 114259 (2019).
42. G.Su, Yu.Pan, Ya.Zhang et al., *Energy*, **113**, 723 (2016).
43. Z.Xiang, Ya.Lu, X.Gong et al., *J. Hazard. Mater.*, **173**, 243 (2010).
44. I.Iliuta, F.Larachi, *Int. J. of Greenhouse Gas Control*, **79**, 1 (2018).
45. A.C.N.Preller, *North-West University: Potchefstroom*, 138 (2011).
46. S.Sahin, F.Sefidvash, *Energy Convers. Manag.*, **49**, 1902 (2008).
47. I.Barna, Ya.Gumnytskyi, V.Atamanyuk, *Chem. Chem. Technol.*, **7**, 461 (2013).
48. R.Hosovskyi, D.Kindzera, V.Atamanyuk, *Chem. Chem. Technol.*, **10**, 460 (2016).
49. V.Atamaniuk, I.Huzova, Z.Hnativ, *Chem. Chem. Technol.*, **12**, 263 (2018).
50. T.Zeiser, M.Steven, H.Freun et al., *Phil. Trans. R. Soc. Lond. A*, **360**, 507 (2002).
51. L.Davidson, Chalmers University of Technology: Goteborg, Sweden, 50 (2016).
52. O.Kuntyi, O.Dobrovetska, S.Korniy et al., *Functional Materials*, **27**, 277 (2020).
53. A.Koekemoer, A.Luckos, *Fuel*, **158**, 232 (2015).
54. D.Janecki, A.Burghardt, Gr.Bartelmus, *Chem. Engin. J.*, **237**, 176 (2014).
55. V.Atamanyuk, Ya.Gumnytskyi, Monograph, Lviv Polytechnic Publishing House, Lviv (2013).
56. R.Havryliv, V.Maystruk, *Chem. Chem. Technol.*, **11**, 71 (2017).